Palestine Journal of Mathematics

Vol. 2(2) (2013) , 243–264

Spectral Behavior of Elastic Beam Models with Monotone and Non-Monotone Feedback Boundary Conditions

Richard J. Marchand and Timothy J. McDevitt

Communicated by Irena Lasiecka

MSC 2010: 35, 93, 74

Keywords and phrases: beam equations with non-monotone feedback boundary conditions, flexible robot arms, nondissipative boundary conditions, Gevrey's class, stability, spectral analysis

Abstract. The primary goal of this paper is to present results related to the stability of elastic beam models incorporating non-monotone boundary conditions with applications involving flexible robot manipulators. Unlike monotone boundary conditions which give rise to a dissipative energy law, the classical energy formulation associated with elastic beams employing non-monotone boundary conditions does not explicitly guarantee that the energy is dissipative. That condition naturally gives rise to questions of stability and even well-posedness of finite energy solutions. The Euler-Bernoulli beam has been studied extensively in the literature and a recent paper by Guiver and Opmeer [11] demonstrates a *lack of stability* for the closely related Rayleigh and Timoshenko beam models. We extend their results here by proving the well-posedness of the Rayleigh model and provide a more extensive and illuminating computational analysis of the spectra associated with four related beam models (Euler-Bernoulli, Timoshenko, shear, and Rayleigh.) The analyses demonstrate significant differences in the spectra of each model, thereby suggesting different stability properties. We also show that even though there are infinitely many (high frequency) unstable modes for the Rayleigh and Timoshenko models, most if not all (low frequency modes) related to physical applications of these models are stable.

1 Introduction

In the past few decades a great deal of attention has been given to the modeling, simulation, and control of flexible robot arms and linkages. Among the many advantages flexible robots enjoy over their rigid counterparts is higher speed, lighter weight, greater manueverability, high payload to weight ratios, lower power consumptions, safer working environment, and the ability to work in hazardous environments. Their low weight makes flexible manipulators ideal for space applications such as the 17.6 m manipulator on the International Space Station. Large manipulators are also employed to inspect hazardous waste storage facilities in which the manipulators must be able to fit into a hole that is 0.1 to 1 m in diameter with a reach of 25 m or more [2]. In addition to applications in space and hazardous waste, flexible robot manipulators are also used in high speed industrial automation, large scale construction, mining, surface inspection in large structures such as airplanes/submarines, etc. The trade-off for these advantages is that it is difficult to control the tip of the arm due to structural flexibility in the arm segments and linkages, and increased susceptibility to vibrations, especially in low weight, high speed applications. For a good summary of the current state of research applied to flexible manipulators see the books [1, 2, 3].

Stabilizing oscillations in the arms can often be achieved most simply and with the fewest actuators and sensors by applying a boundary control at the root of the arm. Luo and Guo [6] specifically consider an Euler-Bernoulli beam with feedback of the form

$$y_{tt}(x,t) + y_{xxxx}(x,t) = -x\theta''(t) - s''(t), \qquad x \in (0,1) \tag{1.1}$$

along with suitable initial and boundary conditions $y(0,t) = y'(0,t) = y''(1,t) = y'''(1,t) = 0$. The control is applied at $x = 0$, where θ'' and s'' are the angular and linear accelerations of the base, respectively. Measuring the bending strain rate $y_{xxt}(0,t)$ and the shear strain rate $y_{xxxt}(0,t)$ at the base, they consider, with slightly different notation, the feedback laws

$$\theta''(t) = \bar{k}_s y_{xxt}(0,t) - k_s y_{xxxt}(0,t) \qquad s''(t) = -\bar{k}_m y_{xxxt}(0,t), \tag{1.2}$$

where $\bar{k}_s, \bar{k}_m, k_s \geq 0$. Making the change of variable $u(x,t) = y_{xx}(1-x,t)$ leads to a homogeneous beam equation

$$u_{tt} + u_{xxxx} = 0 \tag{1.3}$$

with boundary conditions

$$u(0,t) = u_x(0,t) = 0, \qquad u_{xx}(1,t) + \bar{k}_m u_{xt}(1,t) = 0, \quad u_{xxx}(1,t) - \bar{k}_s u_t(1,t) - k_s u_{xt}(1,t) = 0.$$

Multiplying by u_t leads to the energy relation

$$\frac{d}{dt}\int_0^1 \frac{1}{2}\left(u_t^2 + u_{xx}^2\right) dx = -\bar{k}_m u_t(1,t)^2 - \bar{k}_s u_{xt}(1,t)^2 - k_s u_{xt}(1,t) u_t(1,t), \tag{1.4}$$

which is clearly dissipative if $k_s = 0$ in which case the boundary conditions are called monotone. The novelty occurs precisely for non-monotone boundary conditions when $k_s > 0$ because it is not obvious from (1.4) that the energy is dissipated. Here and throughout this paper, the gain parameters in the boundary conditions are identified by a k with a subscript of m if feedback is applied to the moment and a subscript of s if the feedback is applied to the shear. Moreover, to distinguish between monotone and non-monotone boundary conditions, gain parameters that involve monotone boundary conditions are indicated with an overbar ($\bar{\ }$). A more general version of this model is presented below.

The Euler-Bernoulli model is the simplest beam model one can use, but there are other popular models that include more aspects of the relevant physics. See [15] for example. In this paper, we consider the spectral behavior of four related beam models with different monotone and non-monotone boundary conditions: Euler-Bernoulli, Timoshenko, Rayleigh, and shear. Guiver and Opmeer [11] proved the very interesting results that the Rayleigh and Timoshenko models are unstable with non-monotone boundary feedback controls and that there are countably infinite many eigenvalues with positive real part in both cases. Since the Rayleigh and Timoshenko models are often considered to be more faithful models of the real world, their work calls into question the practical use of non-monotone boundary conditions and suggests that the surprising Gevrey regularity of the Euler-Bernoulli model is a happy accident. However, there is more to be said on the subject. For instance, in addition to their proof, the authors of [11] show a portion of the spectrum as in Figure 1 for the Rayleigh model to indicate instability, but the authors appear to have chosen γ, which is defined below in (3.3), to be one. However, as we demonstrate below, in practice γ is very small which implies that all of the physically relevant modes are in fact stable. A similar result holds for the Timoshenko model. We further extend the results of [11] by proving well-posedness of the Rayleigh model.

In what follows, we consider each beam model in turn and demonstrate the radical differences in the spectral behaviors between the four similar models. Known theoretical results are included for each model, but the emphasis is on the numerical nature of the spectra and the relationship to physics. Although we provide accurate estimates for the eigenvalues for all of the models and accompanying boundary conditions, the stability of a partial differential equation (PDE) cannot be determined solely from the location of the spectrum. While it is true that if any eigenvalue has a positive real part, the system has a corresponding unstable mode, it is not possible in general to conclude that a system is stable when all of the eigenvalues reside in the open left-half plane. Indeed, it is well known that the location of the spectrum in the open left-half plane is only a necessary but not sufficient condition for stability for PDEs.

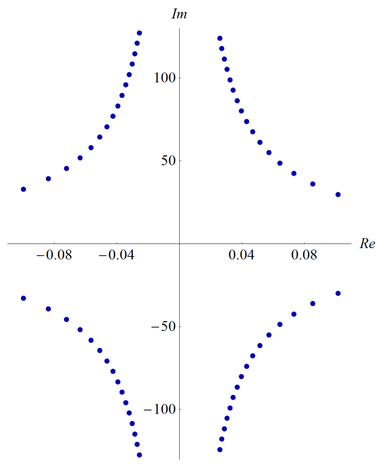

Figure 1. Portion of the spectrum for the Rayleigh beam with non-monotone moment ($\bar{k}_m = \bar{k}_s = k_s = 0$, $k_m = 5$, $\gamma = 1$) boundary conditions.

Our discussion begins with a general study of the Euler Bernoulli Beam model since it is the simplest of the four models yet clearly exhibits the most significant differences between monotone and non-monotone boundary conditions. A careful derivation of the Timoshenko model follows in order to study the physical limitations of the models relative to stability properties. The Euler-Bernoulli, Rayleigh and shear models are special cases of the Timoshenko model.

2 The Euler-Bernoulli Beam

A general form of the Euler-Bernoulli model defined for all $x \in \Omega \equiv (0,1)$, and $t > 0$ is given by

$$u_{xxxx} + u_{tt} = f(x,t). \tag{2.1}$$

with boundary conditions

$$u(0,t) = u_x(0,t) = 0 \tag{2.2}$$

$$\underbrace{u_{xx}(1,t)}_{-M(1,t)} + k_m u_t(1,t) + \bar{k}_m u_{xt}(1,t) = 0 \tag{2.3}$$

$$\underbrace{-u_{xxx}(1,t)}_{S(1,t)} + k_s u_{xt}(1,t) + \bar{k}_s u_t(1,t) = 0, \tag{2.4}$$

where $M(1,t)$ and $S(1,t)$ denote the boundary moment and shear force respectively. The energy given by

$$E(t) = \frac{1}{2}\int_0^1 \left(u_t^2 + u_{xx}^2\right) dx$$

satisfies the relation

$$\frac{d}{dt}E(t) = \int_0^1 f(x,t)dx - (k_m + k_s)u_{xt}(1,t)u_t(1,t) - \bar{k}_m u_{xt}^2(1,t) - \bar{k}_s u_t^2(1,t). \tag{2.5}$$

The finite energy space for this model is $H^2_{cl}(0,1) \times L_2(0,1)$ where

$$H^2_{cl}(0,1) = \left\{v \in H^2(0,1) | v(0) = v_x(0) = 0\right\}$$

.

Boundary control of the Euler-Bernoulli beam has been studied extensively for both monotone and non-monotone boundary conditions. With monotone boundary conditions ($k_m = k_s = 0$), and $f = 0$, the expression in (2.5) clearly shows that the energy is dissipative and the classical methods of dissipative semigroups applies. Indeed, the model in (2.1) with $f = 0$ and moment control ($\bar{k}_s = 0$), generates a contraction semigroup that is exponentially stable. Chen et al. [7] first proved exponential stability of the Euler-Bernoulli system with $\bar{k}_m = k_m = k_s = 0$, $\bar{k}_s > 0$ and [8] proved exponential stability for $k_m = \bar{k}_s = k_s = 0$, $\bar{k}_m > 0$. A similar result is also true in the case of plates where the analysis is much more technical [20, 21].

However, with non-monotone boundary conditions, $k_m > 0$ or $k_s > 0$, there is no apparent dissipation in the energy expression (2.5). Moreover, the boundary terms do not exhibit any information regarding additional boundary regularity of solutions which is always the case in problems with monotone boundary dissipation, and they display an unboundedness on the boundary which is not controlled by the energy. These issues have caused some researchers to rely on Reisz basis techniques as in [9] in which exponential stability was proven in the case of non-monotone shear control, $k_m = \bar{k}_m = \bar{k}_s = 0$, $k_s > 0$. For non-monotone moment control, $\bar{k}_m = k_s = \bar{k}_s = 0$, $k_m > 0$, [5] used Reisz basis methods to show that the resulting semigroup of the dual problem is of Gevrey's class. A more general approach for achieving that same result was given in [12] which used microlocal analysis. In particular, consider the operator $A : D(A) \subset H \to H$ given by

$$A(u, v) = (v, -u_{xxxx})$$

$$D(A) \equiv \{u \in H^2_{cl}(0,1) \cap H^4(0,1), v \in H^2_{cl}(0,1),\ u_{xxx}(1) = 0, u_{xx}(1) = -k_m v(1)\}.$$

Belinskiy and Lasiecka [12] showed that the semigroup e^{At} is of Gevrey's class with the following approximation for the higher modes:

$$\lambda_n \approx \begin{cases} -\frac{(2n-1)\pi}{2}\ln\left(\frac{1+k_m}{1-k_m}\right) \pm i\left[\frac{(2n-1)^2\pi^2}{4} - \frac{1}{4}\ln^2\left(\frac{1+k_m}{1-k_m}\right)\right] & 0 \le k_m < 1 \\ -n\pi\ln\left(\frac{k_m+1}{k_m-1}\right) \pm i\left[n^2\pi^2 - \frac{1}{4}\ln^2\left(\frac{k_m+1}{k_m-1}\right)\right] & k_m > 1 \end{cases} \tag{2.6}$$

and for $k_m = 1$, we have the exact result that

$$\lambda_n = -\left[\frac{(2n-1)\pi}{2}\right]^2, \quad n \in \mathbb{N}.$$

Asymptotically, the imaginary parts are roughly proportional to the square of the (negative) real parts, which implies strong damping of the higher modes. Therefore, the non-monotone damping provides surprisingly good decay rates.

The use of microlocal analysis has also been employed to address multidimensional problems, see [13].

2.1 Numerical Results for the Euler-Bernoulli Beam

Extensive numerical results are given in [14], but we reproduce some of those results here for easy comparison with the other theories. Figure 2 shows the spectral behavior of the Euler-Bernoulli beam with monotone ($k_m = k_s = 0$) boundary conditions. Like the shear and Rayleigh models, the eigenvalues for moment control ($\bar{k}_m > 0$, $\bar{k}_s = 0$) move clockwise above the real axis and the eigenvalues for shear control ($\bar{k}_m = 0$, $\bar{k}_s > 0$) move counter-clockwise. One notable distinction of the Euler-Bernoulli theory is that the eigenvalues are quadratically spaced instead of linearly spaced which is the case in the other models, and this is a well-known feature of the Euler-Bernoulli model.

Figure 3 shows the spectral behavior for non-monotone moment control ($\bar{k}_m = \bar{k}_s = k_s = 0$, $k_m > 0$). The paths in this case are very different than those elsewhere in this paper. Each complex

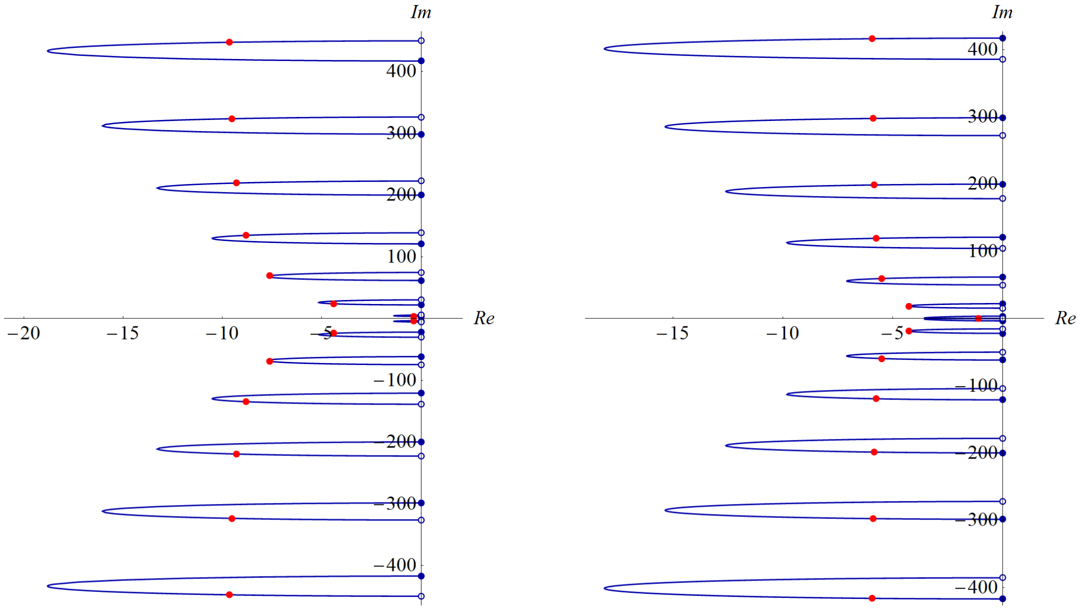

Figure 2. Portion of the spectrum for the Euler-Bernoulli beam with monotone moment (left, $\bar{k}_s = k_m = k_s = 0$, $\bar{k}_m = 0.1$) and shear (right, $\bar{k}_m = k_m = k_s = 0$, $\bar{k}_s = 3$) boundary conditions along with the paths that the eigenvalues take as the gain parameter increases from zero (disks) to infinity (open circles).

conjugate pair of eigenvalues becomes real for $k_m = 1$. For values of k_m slightly more than one, each pair of eigenvalues is real with one moving left and the other moving right along the real axis. For k_m slightly larger still, they become complex again and move back toward the imaginary axis as $k_m \to \infty$. (This unusual behavior is discussed in more detail in [14].) The sample set of eigenvalues indicated in Figure 3 correspond to $k_m = 0.99999999$. Note how far the higher eigenvalues have to move to reach the real axis for $k_m = 1$. This demonstrates how sensitive the spectrum is to the chosen value of k_m and it highlights again the need for increased precision in the calculations.

3 The Timoshenko Beam

In order to adequately incorporate more of the relevant physics associated with beams that is not captured in the Euler-Bernoulli model, it is necessary to recall the basic equations of motion and constitutive laws that lead to their development. To this end, we consider models for a long, homogeneous beam of length L with density ρ, constant cross-sectional area A, moment of inertia about the principal axis I, Young's and shear moduli E and G, respectively, and shear factor k that depends on the shape of the cross section of the beam. Let U be a representative transverse displacement, let Lx be the axial variable, and let $L^2\sqrt{\rho A/(EI)}t$ be time. If $Uu(x,t)$ is the displacement of the beam and $(U/L)\alpha(x,t)$ is the angle of rotation, then the dimensionless equations of motion are

$$\frac{\partial^2 u}{\partial t^2} - \frac{\partial S}{\partial x} = p(x,t) \tag{3.1}$$

$$\gamma\frac{\partial^2 \alpha}{\partial t^2} + \frac{\partial M}{\partial x} - S = m(x,t) \tag{3.2}$$

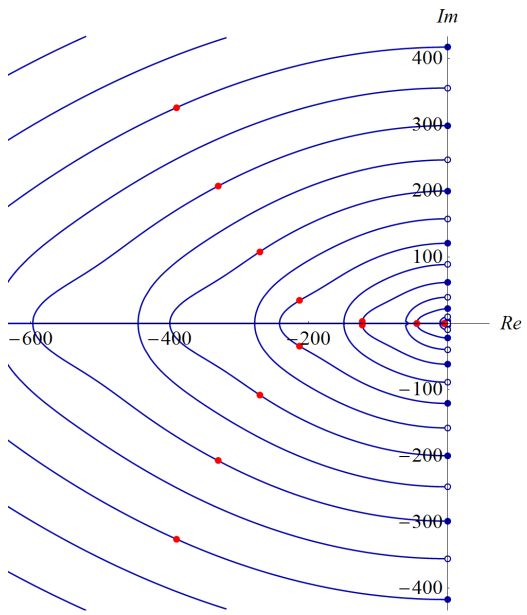

Figure 3. Portion of the spectrum for the Euler-Bernoulli beam with non-monotone moment ($\bar{k}_m = \bar{k}_s = k_s = 0$, $k_m = 0.99999999$) boundary conditions along with the paths that the eigenvalues take as the gain parameter increases from zero (disks) to infinity (open circles). If $k_m = 1$, then *all* of the eigenvalues are real and negative.

where $(EIU/L^2)M(x,t)$ is the moment, $(EIU/L^3)S(x,t)$ is the shear force, $(EIU/L^4)p(x,t)$ is an applied transverse force per unit length, $(EIU/L^3)m(x,t)$ is an applied moment per unit length,

$$\gamma = \frac{I}{AL^2}, \qquad \text{and} \qquad g = \left(\frac{kG}{E}\right)\frac{1}{\gamma}. \tag{3.3}$$

For a linearly elastic material, we have the constitutive laws

$$M = -\frac{\partial \alpha}{\partial x} \qquad \text{and} \qquad S = g\left(\frac{\partial u}{\partial x} - \alpha\right). \tag{3.4}$$

Substituting (3.3) and (3.4) into (3.1) and (3.2) yields the equations of motion of Timoshenko beam theory:

$$u_{tt} - g\left(u_{xx} - \alpha_x\right) = p \tag{3.5}$$

$$\gamma\alpha_{tt} - \alpha_{xx} - g\left(u_x - \alpha\right) = m, \tag{3.6}$$

where $(u, u_t, \alpha, \alpha_t) \in H^2(0,1) \times H^1(0,1) \times H^2(0,1) \times H^1(0,1)$. With sufficient additional regularity, the system (3.5)-(3.6) can be written in terms of displacement alone as

$$u_{xxxx} - \left(\frac{1}{g} + \gamma\right) u_{xxtt} + \frac{\gamma}{g} u_{tttt} + u_{tt} = f(x,t), \tag{3.7}$$

which factors as

$$\left(\frac{\partial^2}{\partial x^2} - \gamma\frac{\partial^2}{\partial t^2}\right)\left(\frac{\partial^2}{\partial x^2} - \frac{1}{g}\frac{\partial^2}{\partial t^2}\right) u + u_{tt} = f(x,t), \qquad 0 < x < 1,$$

where

$$f(x,t) := \frac{\gamma}{g} p_{tt}(x,t) - \frac{1}{g} p_{xx}(x,t) - m_x(x,t) + p(x,t).$$

However, working with displacements alone, as in (3.7), is inconvenient when we consider the boundary conditions, at least one of which must include α. Specifically, at each end, we can specify either u or $S = g(u_x - \alpha)$ and either α or $M = -\alpha_x$.

Using u_t and α_t as multipliers for (3.5) and (3.6), respectively, we obtain the following general energy relationship:

$$\frac{d}{dt} E_{\gamma,g}(t) = \int_0^1 (pu_t + m\alpha_t)\, dx + \left. (Su_t - M\alpha_t) \right|_0^1, \tag{3.8}$$

where the total energy

$$E_{\gamma,g}(t) = \int_0^1 \frac{1}{2} \left[\underbrace{u_t^2 + \gamma \alpha_t^2}_{kinetic} + \underbrace{\alpha_x^2}_{bending} + \underbrace{g\,(u_x - \alpha)^2}_{shear} \right] dx. \tag{3.9}$$

The subscripts γ and g will vary depending on which beam theory we are considering. For a Timoshenko beam, $\gamma, g > 0$. To recover the Euler-Bernoulli beam, we set $\gamma = 0$ and let $g \to \infty$, so that there is no moment of inertia or shear effects, and $\alpha = u_x$.

We take the beam to be clamped at the left end, and at the right end we impose boundary feedback controls on the moment and shear.

$$u(0,t) = \alpha(0,t) = 0 \tag{3.10}$$

$$\underbrace{\alpha_x(1,t)}_{-M(1,t)} + k_m u_t(1,t) + \bar{k}_m \alpha_t(1,t) = 0, \qquad k_m, \bar{k}_m \geq 0 \tag{3.11}$$

$$\underbrace{g\,(u_x(1,t) - \alpha(1,t))}_{S(1,t)} + k_s \alpha_t(1,t) + \bar{k}_s u_t(1,t) = 0, \qquad k_s, \bar{k}_s \geq 0. \tag{3.12}$$

The resulting energy relationship is

$$\frac{d}{dt} E_{\gamma,g}(t) = \int_0^1 (pu_t + m\alpha_t)\, dx - (k_m + k_s)\alpha_t(1,t) u_t(1,t) - \bar{k}_m \alpha_t^2(1,t) - \bar{k}_s u_t^2(1,t). \tag{3.13}$$

If we set the applied loads $p = m = 0$ and all four gain parameters to zero ($\bar{k}_m = \bar{k}_s = k_m = k_s = 0$), then the energy is conserved and we recover the standard problem of a cantilevered beam, clamped at $x = 0$ and free at $x = 1$. For *monotone* boundary conditions $k_m = k_s = 0$, we have

$$\frac{d}{dt} E_{\gamma,g}(t) = -\bar{k}_m u_{xt}^2(1,t) - \bar{k}_s u_t^2(1,t) \leq 0,$$

so the energy is clearly dissipative. In contrast, the *non-monotone* boundary conditions, $\bar{k}_m = \bar{k}_s = 0$, give

$$\frac{d}{dt} E_{\gamma,g}(t) = -(k_m + k_s)\alpha_t(1,t) u_t(1,t),$$

in which case it is not clear whether or not the energy is dissipative as was the case for the Euler-Bernoulli model, in (2.1)–(2.4). The specific problem with $\bar{k}_m = \bar{k}_s = k_s = 0$ is dual to the problem with $\bar{k}_m = \bar{k}_s = k_m = 0$, so we set $k_s = 0$ in our examples for simplicity.

In general, well-posedness of finite energy solutions $(u, u_t, \alpha, \alpha_t)$ is considered in the finite energy space $H \equiv H^1_{pl}(0,1) \times L_2(0,1) \times H^1_{pl}(0,1) \times L_2(0,1)$, where $H^1_{pl}(0,1) = \{ v \in H^1(0,1) | v(0) = 0 \}$.

For the monotone boundary conditions, well-posedness is typically established by showing that the system generates an appropriate semigroup as in [10]. However, the non-monotone boundary conditions ruin the dissipative properties of the underlying generator and calls into question the existence of a dissipative energy law.

Before proceeding to our results, we want to emphasize that all of the beam models considered in this paper have a common set of assumptions. Han et al. give a list of six assumptions on p. 928 of [15] that we do not repeat here in its entirety. Nevertheless, one of those assumptions is that the beam is very long, which means that the thickness of the beam should be small in comparison to its length. Since we have not specified the cross-sectional geometry of the beam, we use the radius of gyration $\sqrt{I/A}$ as a rough measure of the thickness. Therefore, for a beam model to apply to a physical reality, $\sqrt{\gamma} = \sqrt{I/A}/L$ must be very small. In fact, Han et al. [15] call $1/\sqrt{\gamma}$ the slenderness ratio of the beam. Consequently, because of (3.3), g must also be very large.

As an example, let us consider a beam with a circular cross section composed of an isotropic material. In that case, $E = 2(1+\nu)G$ where $-1 \le \nu \le 1/2$ is Poisson's ratio. If the radius is R, then $k = 6(1+\nu)/(7+6\nu)$, $I = \pi R^4/4$, and $A = \pi R^2$. Using $\nu = 1/3$, which is appropriate for typical engineering materials like copper, then

$$\gamma = \left(\frac{R}{2L}\right)^2 \qquad \text{and} \qquad g = \frac{3}{\gamma}.$$

For a long beam, $R/L \ll 1$, so γ and $1/g$ are both very small and are comparable in size. In the numerical results that follow, we take $g = 3/\gamma$ for simplicity.

The three other beam theories considered in this paper can be derived from the Timoshenko theory by choosing extreme values for γ and g: the Euler-Bernoulli beam ($\gamma = 0$, $g = \infty$), the Rayleigh beam ($g = \infty$), and the shear beam ($\gamma = 0$). It was first demonstrated by Timoshenko [19] that, in our notation, γ and $1/g$ are of comparable size. Nevertheless, all four theories are still used and studied today.

One final limitation of beam theories is that they are no longer adequate models of reality if the wavelengths are comparable in size to the thickness of the beam. For very high frequencies, a two or three-dimensional elasticity theory is necessary. In an attempt to quantify the practical limits of our analysis, consider a beam that is simply supported ($u = \alpha_x = 0$) at both ends. In that case, solutions of the form $e^{i\omega t}\sin(n\pi x)$, $n \in \mathbb{N}$, are appropriate and the corresponding wavelength is $2L/n$. Measuring the beam thickness with $\sqrt{\gamma}L$, we conclude that beam theories become inappropriate for $n = \mathcal{O}(1/\sqrt{\gamma})$. For the simply supported Euler-Bernoulli beam, $\omega = (n\pi)^2$, for the Rayleigh beam, $\omega \approx n\pi/\sqrt{\gamma}$ for large n, for the shear beam, $\omega \approx n\pi\sqrt{g}$ for large n, and for the Timoshenko beam, $\omega \approx n\pi/\sqrt{\gamma}, n\pi\sqrt{g}$ for large n. We can conclude that, roughly, beam eigenvalues are not reliable if the imaginary part of the eigenvalue is $\mathcal{O}(1/\gamma)$ or $\mathcal{O}(\sqrt{g/\gamma})$.

3.1 Numerical Results for the Timoshenko Beam

Solutions of the form

$$u(x,t) = r_+ e^{\lambda t}\left\{c\left[r_+\left(\frac{1}{g}\lambda^2 - r_-^2\right)\sinh(r_+ x) + r_-\left(r_+^2 - \frac{1}{g}\lambda^2\right)\sinh(r_- x)\right] + \right.$$
$$\left. r_-\left(r_+^2 - \frac{1}{g}\lambda^2\right)\cosh(r_- x) + r_-\left(\frac{1}{g}\lambda^2 - r_+^2\right)\cosh(r_+ x)\right\} \qquad (3.14)$$

and

$$\alpha(x,t) = \frac{1}{g}e^{\lambda t}\left(\frac{1}{g}\lambda^2 - r_+^2\right)\left[-cr_+\left(r_-^2 - \frac{1}{g}\lambda^2\right)\cosh(r_-x) + cr_+\left(r_-^2 - \frac{1}{g}\lambda^2\right)\cosh(r_+x) - \right.$$
$$\left. r_-^2 r_+ \sinh(r_-x) + r_- r_+^2 \sinh(r_+x) - \frac{1}{g}\lambda^2 r_- \sinh(r_+x) + \frac{1}{g}\lambda^2 r_+ \sinh(r_-x)\right] \quad (3.15)$$

where $c \in \mathbb{C}$ and

$$r_\pm = \sqrt{\frac{1}{2}\lambda\left[\left(\frac{1}{g}+\gamma\right)\lambda \pm \sqrt{\lambda^2\left(\frac{1}{g}-\gamma\right)^2 - 4}\right]}$$

satisfy the PDEs (3.6) and the clamped boundary conditions (3.10) at $x = 0$ provided that $\lambda \neq 0, \pm 2/|(1/g) - \gamma|, \pm i\sqrt{g/\gamma}$. For simplicity we apply the monotone and non-monotone boundary conditions (3.11) and (3.12) separately. In the monotone ($k_m = k_s = 0$) case, the feedback boundary conditions at the right end give the following transcendental equation for the eigenvalues.

$$\bar{A} + \bar{B}\bar{k}_m + \bar{C}\bar{k}_s + \bar{D}\bar{k}_m\bar{k}_s = 0 \quad (3.16)$$

where

$$\bar{A} = 2\left[-\lambda^2\left(\gamma + \frac{1}{g}\right)\sinh(r_-)\sinh(r_+) + r_-r_+\cosh(r_-)\cosh(r_+)\left(\lambda^2\left(\frac{1}{g}-\gamma\right)^2 - 2\right) - 2r_-r_+\right],$$

$$\bar{B} = \lambda\left[r_+\sinh(r_-)\cosh(r_+)\left(\lambda^2\left(\frac{1}{g}-\gamma\right)^2 + \left(r_+^2 - r_-^2\right)\left(\frac{1}{g}-\gamma\right) - 4\right)\right.$$
$$\left. + r_-\cosh(r_-)\sinh(r_+)\left(\lambda^2\left(\frac{1}{g}-\gamma\right)^2 - \left(r_+^2 - r_-^2\right)\left(\frac{1}{g}-\gamma\right) - 4\right)\right],$$

$$\bar{C} = \frac{1}{\lambda}\left(r_-^2 - r_+^2\right)\left[r_-\cosh(r_-)\sinh(r_+)\left(2 - \frac{\lambda^2}{g^2} + \frac{\gamma\lambda^2 + r_-^2 - r_+^2}{g}\right) - \right.$$
$$\left. r_+\sinh(r_-)\cosh(r_+)\left(2 - \frac{\lambda^2}{g^2} + \frac{\gamma\lambda^2 - r_-^2 + r_+^2}{g}\right)\right],$$

and

$$\bar{D} = 2\left[\lambda^2\sinh(r_-)\sinh(r_+)\left(\gamma - \frac{3}{g} + \frac{\lambda^2}{g}\left(\frac{1}{g}-\gamma\right)^2\right) - 2r_-r_+\cosh(r_-)\cosh(r_+) + 2r_-r_+\right].$$

Likewise, the non-monotone ($\bar{k}_m = \bar{k}_s = 0$) boundary conditions give

$$A + B(k_m + k_s) + Ck_mk_s = 0 \quad (3.17)$$

where

$$A = r_-r_+\cosh(r_-)\cosh(r_+)\left[\lambda^2\left(\frac{1}{g}-\gamma\right)^2 - 2\right] - \lambda^2\left(\gamma + \frac{1}{g}\right)\sinh(r_-)\sinh(r_+) - 2r_-r_+,$$

$$B = \left(\frac{1}{g} - \gamma\right) \lambda r_- r_+ + \lambda \left[\frac{1}{g}\lambda^2 \left(\frac{1}{g} - \gamma\right) - 2\right] \sinh(r_-)\sinh(r_+) + \lambda r_- r_+ \left(\gamma - \frac{1}{g}\right) \cosh(r_-)\cosh(r_+),$$

and

$$C = -\lambda^2 \sinh(r_-)\sinh(r_+) \left[\gamma - \frac{3}{g} + \frac{\lambda^2}{g^2}\left(\frac{1}{g} - 2\gamma\right) + \frac{1}{g}\gamma^2\lambda^3\right] + 2r_- r_+ \cosh(r_-)\cosh(r_+) - 2r_- r_+.$$

Note that the form of (3.17) shows that the eigenvalues are the same for $\bar{k}_m = \bar{k}_s = k_m = 0$ and $\bar{k}_m = \bar{k}_s = k_s = 0$, as mentioned above. Again, for simplicity, we set $k_s = 0$ in our examples.

Solving either (3.16) or (3.17) is simply a matter of root-finding, but there can be considerable difficulty in finding suitable initial guesses in some cases. If all of the gain parameters are zero, then all of the eigenvalues are purely imaginary and both equations (3.16) or (3.17) are relatively easy to solve. Those solutions are used as initial guesses for problems where one of the gain parameters is incremented. Continuing this process allows us to find the eigenvalues in general. We note that in some situations, especially the non-monotone ones, the eigenvalues change considerably for even the smallest of changes in the corresponding gain parameter, so great care and high precision were necessary. All calculations were done in *Mathematica* with 50 decimal digits of precision.

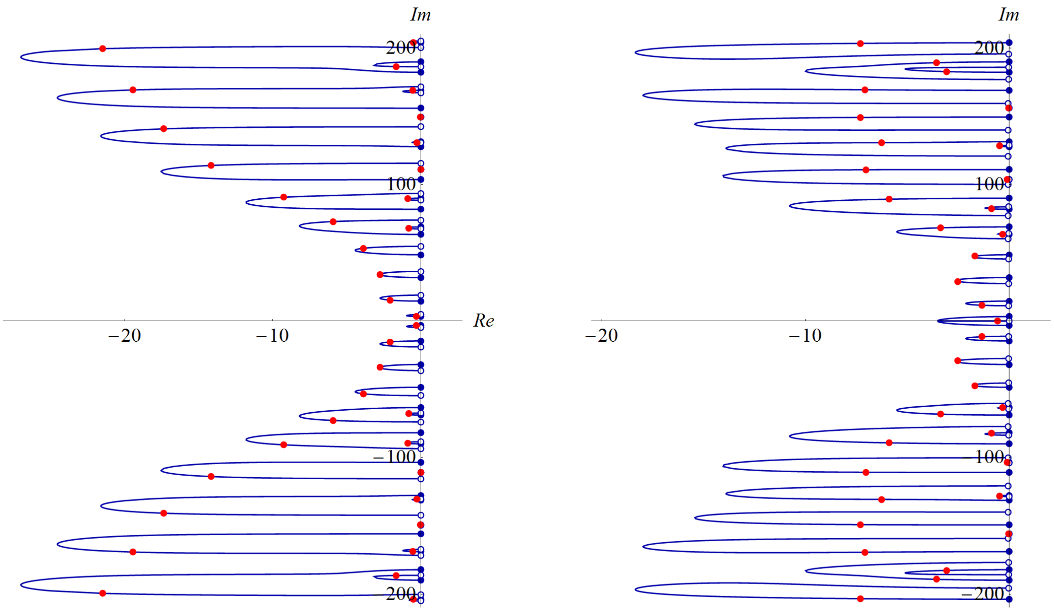

Figure 4. Portion of the spectrum for the Timoshenko beam with monotone moment (left, $\bar{k}_m = 0.1$, $\bar{k}_s = k_m = k_s = 0$, $\gamma = 0.01$, $1/g = 0.03$) and shear (right, $\bar{k}_m = k_m = k_s = 0$, $\bar{k}_s = 5$, $\gamma = 0.01$, $1/g = 0.03$) boundary conditions along with the paths that the eigenvalues take as each gain parameter increases from zero (filled) to infinity (open).

Kim and Renardy [10] proved exponential stability for the Timoshenko beam with monotone ($k_m = k_s = 0$) boundary conditions and samples of the spectra are shown in Figure 4. The choice of $\gamma = 0.01$ is unrealistically large, but smaller values of γ make the figures too busy to be easily understood. The curves start on the imaginary axis at the filled circles and finish on the imaginary axis at the open circles. The connecting curves indicate the paths taken by each eigenvalue as the gain parameter increases from 0 to ∞. In both the monotone moment and monotone shear control cases, the eigenvalues move into the left half-plane, some along clockwise and some along counter-clockwise paths, with their complex conjugate pairs moving in the opposite way. Some of the eigenvalues move much further to the left than others, which is a unique feature of the Timoshenko model, and is a result of the presence of both rotary and shear waves. In both cases, there appear to be modes that are not damped, but close examination reveals that the real parts are very small but negative for $0 < \bar{k}_m < \infty$.

In contrast to the monotone case, Guiver and Opmeer [11] proved that the Timoshenko beam is unstable with non-monotone controls, but they did not publish any graphs of the spectra. Figure 5 shows two such graphs for non-monotone moment control. All of the paths begin on the imaginary axis where $k_m = 0$, but some move into the left and some into the right half-plane. Some of the paths return to the imaginary axis as in the monotone case, but some curves very curiously do not seem to turn around. The graphs also suggest that there are an infinite number of unstable modes, which was actually proved in [11]. However, it is important to note that the lower modes all appear to be stable, so it is possible that all physically relevant modes are actually stable and that the unstable ones are not adequately modeled by the beam theory. Using our criterion that frequencies are suspect when they are $\mathcal{O}(1/\gamma)$ suggests that eigenvalues with imaginary parts less than 100 in magnitude are adequately modeled, so there still appear to be a few unstable modes. However, our criterion is only a rough estimate and further study would be necessary to determine whether or not the suspect modes are adequately modeled by the Timoshenko theory.

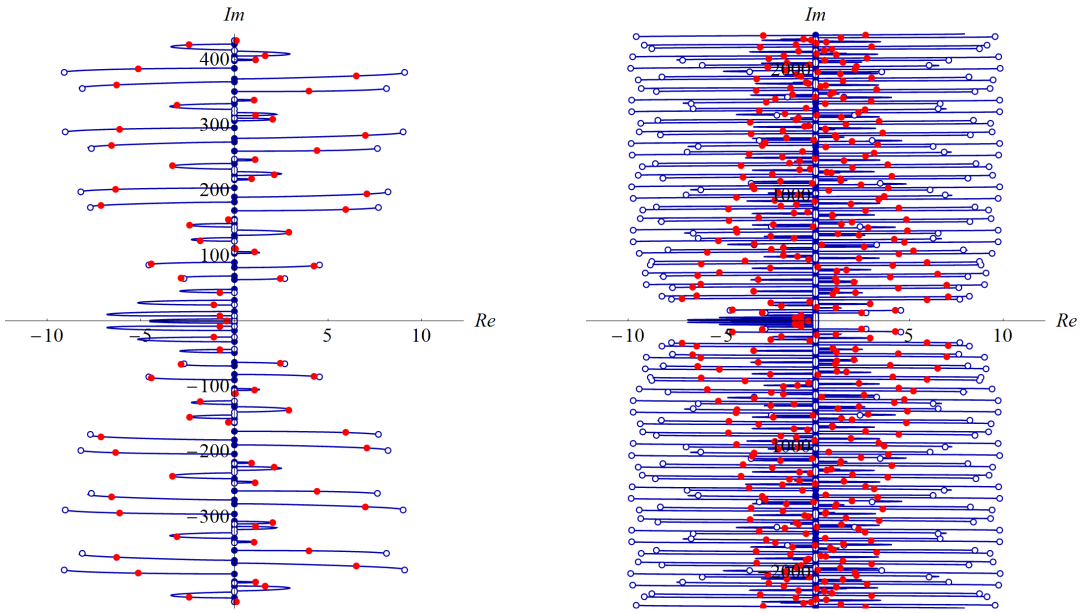

Figure 5. Portion of the spectrum for the Timoshenko beam with non-monotone moment ($\bar{k}_m = \bar{k}_s = k_s = 0$, $k_m = 5$, $\gamma = 0.01$, $1/g = 0.03$) boundary conditions along with the paths that the eigenvalues take as the gain parameter increases from zero (disks) to infinity (open circles). Both graphs contain the same information but are displayed on different vertical scales. Note the large number of unstable modes.

We recall that choosing $\gamma = 0.01$ in Figure 5 is artificially large, so what happens for more realistic values of γ? Figure 6 shows the magnitude of the imaginary part of the first unstable eigenvalue as a function of $1/\gamma$ for ($k_m > 0$). The graph appears to be roughly straight and it has an approximate least-squares slope of 0.579, so our rough criterion of requiring $\omega < 1/\gamma$ suggests that the Timoshenko model does have unstable modes that are adequately modeled by the theory. However, certainty will require a study that applies a higher dimensional elasticity theory or empirical evidence.

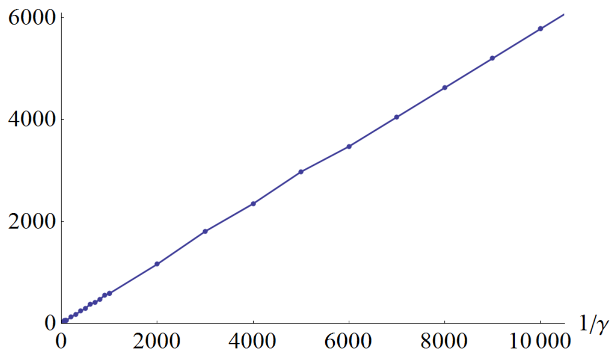

Figure 6. Graph of the magnitude of the imaginary part of the first unstable eigenvalue (for $k_m > 0$, $\bar{k}_m = \bar{k}_s = k_s = 0$) for the Timoshenko model (with $g = 3/\gamma$) as a function of $1/\gamma$. The slope of the line is approximately 0.579.

4 The Shear Beam

The equations for the shear beam were first proposed by Rankine [17] and they can be formally obtained from the Timoshenko equations by ignoring the relationship between γ and g (3.3) and setting $\gamma = 0$ while holding g constant. In equations (3.5) and (3.6), dropping the rotary inertia term gives

$$u_{tt} - g\left(u_{xx} - \alpha_x\right) = p \tag{4.1}$$

$$\alpha_{xx} + g\left(u_x - \alpha\right) = m \tag{4.2}$$

and the displacement equation (3.7) reduces to

$$u_{xxxx} - \frac{1}{g}u_{xxtt} + u_{tt} = f(x,t). \tag{4.3}$$

The major difference between this and the Timoshenko theory is that (4.3) is only second order in time. The boundary conditions (3.10)-(3.12) remain unchanged from the Timoshenko theory and the resulting energy expression is also very similar,

$$\frac{d}{dt}E_{0,g}(t) = -(k_m + k_s)\alpha_t(1,t)u_t(1,t) - \bar{k}_m\alpha_t^2(1,t) - \bar{k}_s u_t^2(1,t), \tag{4.4}$$

where $E_{\gamma,g}$ is defined in (3.9).

The shear beam model has attracted much less attention in the literature, and to the knowledge of the authors, there are currently no published results demonstrating well-posedness or exponential stability for the model. Nevertheless, in spite of the similarities to the Timoshenko model, the behavior of the shear beam is dramatically different. In the monotone shear ($\bar{k}_m = k_m = k_s = 0$, $\bar{k}_s > 0$) case, the eigenvalues approach a vertical asymptote for both large and small $\bar{k}_s$. Specifically, for small $\bar{k}_s$,

$$\lambda_n = -\bar{k}_s \pm i\frac{(2n-1)\pi}{2}\sqrt{g}, \qquad n \in \mathbb{N},$$

and

$$\lambda_n = -g/\bar{k}_s \pm in\pi\sqrt{g}, \qquad n \in \mathbb{N},$$

for large $\bar{k}_s$. This is reminiscent of the spectra of monotone Euler-Bernoulli problems where the eigenvalues line up along a vertical asymptote in the left half-plane as shown in [14]. In contrast, in the monotone moment case ($\bar{k}_s = k_m = k_s = 0$, $\bar{k}_m > 0$), there is no similar asymptotic behavior. However, surprisingly, in the non-monotone case ($\bar{k}_m = \bar{k}_s = k_s = 0$, $k_m > 0$), the eigenvalues are all stable and can be approximated asymptotically as

$$\lambda_n \approx -k_m\sqrt{g} \pm i\left[\frac{(2n-1)\pi\sqrt{g}}{2}\right], \qquad n \in \mathbb{N}, \tag{4.5}$$

for small k_m and

$$\lambda_n \approx -\frac{\sqrt{g}}{k_m} \pm in\pi\sqrt{g}, \qquad n \in \mathbb{N}, \tag{4.6}$$

for large k_m. The apparent stability in this case is radically different from the unstable spectra for the Timoshenko beam with a non-monotone feedback control.

4.1 Numerical Results for the Shear Beam

The transcendental equations (3.16) and (3.17) for the Timoshenko beam apply for the shear beam with $\gamma = 0$ and the solution process is the same as for the Timoshenko beam. Numerical results for the shear beam with monotone boundary conditions are shown in Figure 7 and the eigenvalues all have negative real parts. It is difficult to tell from the graph because the imaginary parts do not change much, but, in the moment case, all of the paths are clockwise above the real axis and counter-clockwise below. In contrast, in the shear case, all of the paths are counter-clockwise above the real axis. Also, the sampled eigenvalues ($\bar{k}_s = 5$) almost look like they lie in a Gevrey sector, but that is just an artifact of the way the graphs are presented.

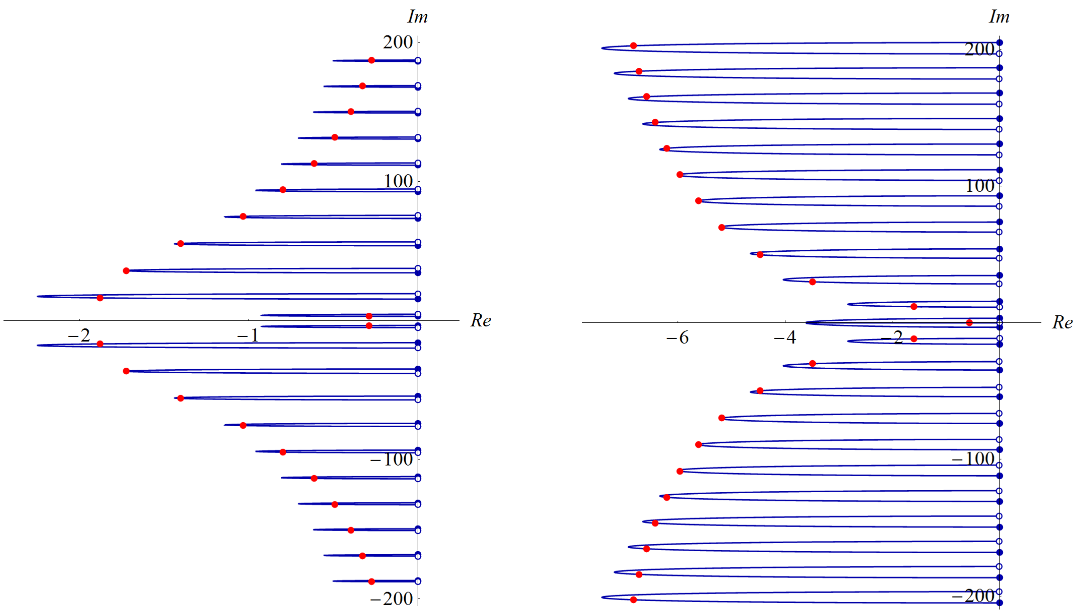

Figure 7. Portion of the spectrum for the shear beam with monotone moment (left, $k_m = \bar{k}_s = k_s = 0$, $\bar{k}_m = 0.1$, $1/g = 0.03$) and shear (right, $\bar{k}_m = k_s = k_m = 0$, $\bar{k}_s = 5$, $1/g = 0.03$) boundary conditions along with the paths that the eigenvalues take as the gain parameter increases from zero (disks) to infinity (open circles).

Figure 8 shows samples of the spectrum for non-monotone moment feedback ($\bar{k}_m = \bar{k}_s = k_s = 0$) for three different values of k_m. For $k_m = 0.5$ the eigenvalues are close to the vertical asymptote given in (4.5). For $k_m = 1$, the visible eigenvalues are close to their left-most extreme points. In the Euler-Bernoulli case [14], the eigenvalues are all real for $k_m = 1$, so the behavior of the shear beam is significantly different. There is one complex conjugate pair of eigenvalues with real part near -180 that become real (and repeated) for a value of k_m slightly higher than 1, and then they stay real with one of them moving off toward negative infinity and the other moving toward the origin. The graph with $k_m = 1.5$ shows that real eigenvalue very close to the origin as well as the asymptotic behavior of the higher eigenvalues as shown in (4.6).

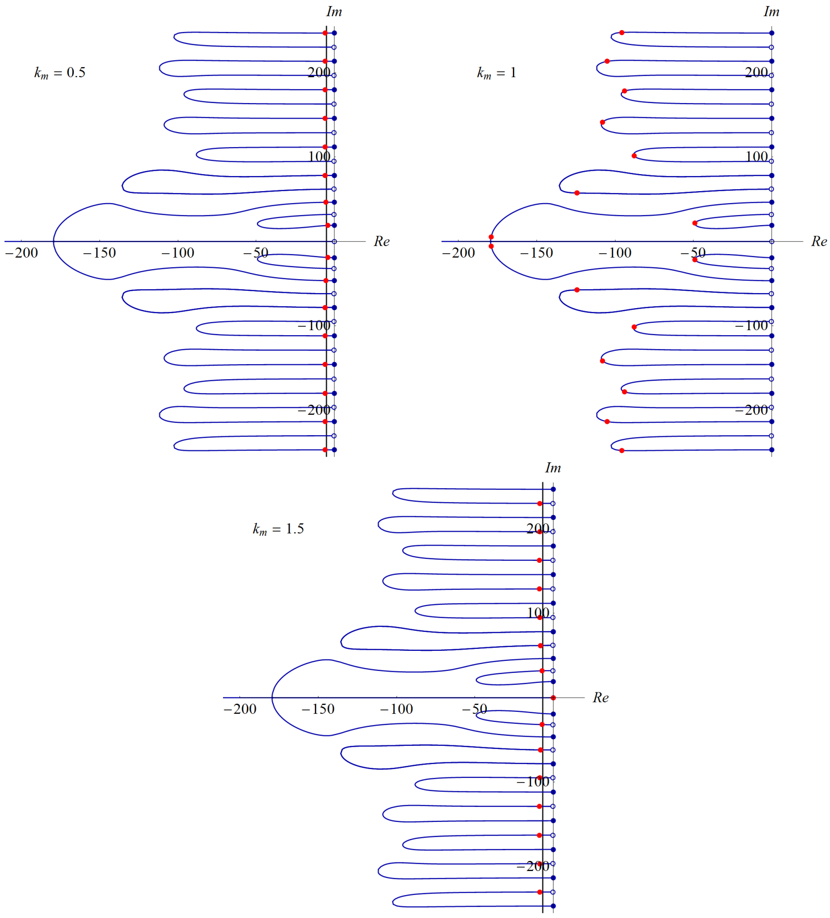

Figure 8. Portion of the spectrum for the shear beam with non-monotone moment ($\bar{k}_m = \bar{k}_s = k_s = 0$ for $k_m = 0.5, 1.0, 1.5$, $1/g = 0.03$) boundary conditions along with the paths that the eigenvalues take as the gain parameter increases from zero (disks) to infinity (open circles).

We emphasize that the shear beam model is very similar to the Timoshenko model – it is obtained by setting a small number (γ) to zero – but, unlike the Timoshenko case, it appears to be stable for all monotone and non-monotone boundary conditions considered herein. The behavior of the shear beam is much more like the Euler-Bernoulli beam than the Timoshenko beam. One additional similarity to the Euler-Bernoulli case is the rapid change of the eigenvalues. The graphs in Figure 8 for $k_m = 0.5$ and $k_m = 1.5$ look very similar. That is because the majority of the eigenvalue paths occur between those two values. It is situations like this that require precision above standard machine precision.

5 The Rayleigh Beam

Lord Rayleigh's model [18] can be obtained from (3.5)-(3.6) by holding γ constant and taking $g \to \infty$ so that there is no shear strain in the beam. Consequently, (3.4) implies that $\alpha = u_x$, so it is quite natural to work only with displacements, in which case (3.7) reduces to

$$u_{xxxx} - \gamma u_{xxtt} + u_{tt} = f(x,t), \tag{5.1}$$

which is structurally the same as the displacement equation for the shear beam (4.3). Unlike the shear beam, however, the boundary conditions can easily be written entirely in terms of u. Specifically, if $m(1,t) = 0$, then

$$u(0,t) = u_x(0,t) = 0 \tag{5.2}$$

$$\underbrace{u_{xx}(1,t)}_{-M(1,t)} + k_m u_t(1,t) + \bar{k}_m u_{xt}(1,t) = 0 \tag{5.3}$$

$$\underbrace{\gamma u_{xtt}(1,t) - u_{xxx}(1,t)}_{S(1,t)} + k_s u_{xt}(1,t) + \bar{k}_s u_t(1,t) = 0 \tag{5.4}$$

The resulting energy expression in the absence of applied loads and moments ($p = m = 0$) is

$$\frac{d}{dt} E_{\gamma,\infty}(t) = -(k_m + k_s)\alpha_t(1,t)u_t(1,t) - \bar{k}_m \alpha_t^2(1,t) - \bar{k}_s u_t^2(1,t), \tag{5.5}$$

where $\alpha = u_x$. For the displacement forms of the Rayleigh and shear models, the energy space is $H^2_{cl}(0,1) \times H^1(0,1)$, where $H^2_{cl}(0,1) = \{v \in H^2(0,1) | v(0) = v_x(0) = 0\}$. The fact that the velocity $u_t \in H^1(0,1)$ makes it possible to obtain well-posedness in the monotone cases using semigroup theory, but well-posedness for the non-monotone cases are not so obvious as we show in the proof of the following theorem.

Theorem 5.1. *The Raleigh Beam* (5.1) *with* $f = 0$ *and any set of boundary feedbacks parametrized by (non-negative)* $k_m, k_s, \bar{k}_m, \bar{k}_s$ *in* (5.2)–(5.4) *generates a strongly continuous semigroup on the finite energy space* $H = H^2_{cl}(\Omega) \times H^1(\Omega)$.

Proof. When k_m, k_s are zero, the problem is monotone and monotone semigroup theory yields the result [22]. Thus it suffices to consider only the case $k_m \neq 0$ or $k_s \neq 0$. By the principle of superposition it is enough to consider each feedback separately.

Let's start with $k_s = 0$. We begin by writing the semigroup representation of the solution

$$M_\gamma u_{tt} + \mathcal{A}u - k_m \mathcal{A} G u_t(1) = 0 \tag{5.6}$$

where $\mathcal{A}u = u_{xxxx}$, $D(\mathcal{A}) = \{u \in H^4(\Omega); u(0) = u_x(0) = 0, u_{xx}(1) = u_{xxx}(1) = 0\}$ and

$$Gg = v, \text{iff } v_{xxxx} = 0, v(0) = v_x(0) = 0, v_{xx}(1) = g, v_{xxx}(1) = 0, \text{(Green's map)}.$$

The map

$$M_\gamma u = u + \gamma A_N u$$

is defined by duality:

$$(M^{1/2} u_t, M^{1/2} v_t) = (u_t, v_t) + \gamma(\nabla u_t, \nabla v_t) \;\; \forall u_t, v_t \in H^1(\Omega),$$

where A_N is the Neumann Laplacian operator, $A_N u = -\Delta u$ with zero Neumann data and N is a classical Neumann map, see [22] page 16 formula (2.4.14). See also [25] page 154. By Green's formula

$$N^* A_N u = u|_\Gamma$$

(see [22]) where the adjoint is taken with respect to L_2 topologies. With the above notation we can write for $U = [u, v]$

$$AU = \begin{bmatrix} 0 & I \\ M_\gamma^{-1}\mathcal{A} & -k_m M_\gamma^{-1}\mathcal{A}GN^*A_N \end{bmatrix} \begin{bmatrix} u \\ v \end{bmatrix}$$

Our goal is to show that A is the generator. To this end we define $A = A_0 + P$ where

$$A_0 U = \begin{bmatrix} 0 & I \\ M_\gamma^{-1}\mathcal{A} & 0 \end{bmatrix} \begin{bmatrix} u \\ v \end{bmatrix},$$

$$PU = \begin{bmatrix} 0 & 0 \\ 0 & -k_m M_\gamma^{-1}\mathcal{A}GN^*A_N \end{bmatrix} \begin{bmatrix} u \\ v \end{bmatrix},$$

It is known that A_0 is a group generator on $H \equiv D(\mathcal{A}^{1/2}) \times D(M^{1/2}) \sim H^2_{cl}(\Omega) \times H^1(\Omega)$ with clamped boundary conditions. In fact, we define

$$(U, \hat{U})_H \equiv (u_{xx}, \hat{u}_{xx}) + (M^{1/2}v, M^{1/2}\hat{v}) = (u_{xx}, \hat{u}_{xx}) + \gamma(\nabla u, \nabla \hat{u})$$

and denote

$$Lg \equiv \int_0^t e^{A_0(t-s)} Bg(s)ds$$

where $Bg \equiv [0, M^{-1}\mathcal{A}G]$. With the above notation the solvability of the abstract evolution

$$U_t = AU$$

is equivalent to the solvability of the integral equation

$$U(t) = e^{A_0 t}U(0) + L(N^*A_N v). \tag{5.7}$$

Lemma 5.2. *The operator*

$$N^*A_N : H^1(\Omega) \to H^{1/2}(\Gamma) \subset L_2(\Gamma)$$

is bounded.

Proof. The result follows from the representation of N^*A_N and associated trace theory. □

Step 1.
The first step in the proof of Theorem 5.1 is to show that L is bounded from

$$L_2(0, T \times \Gamma) \to C(0, T; H).$$

In fact, this (Lemma 5.2) will imply boundedness of the composition $L(N^*A_N) : L_2(0, T; H^1(\Omega)) \to C(0, T; H)$. As a consequence

$$L(N^*A_N P_2) : L_2(0, T; H) \to C(0, T; H) \tag{5.8}$$

which is the key in applying the contraction mapping principle in order to solve the integral equation (5.7). Here P_2 simply means a projection of U on the second coordinate. In view of the above it remains to establish:

Lemma 5.3. *L is bounded from*

$$L_2(0, T \times \Gamma) \to C(0, T; H)$$

Proof. By Green's formula it follows that

$$G^* \mathcal{A} u = \frac{\partial}{\partial \nu} u = u_x(1) \tag{5.9}$$

where the adjoint is taken with respect to L_2 topologies.

Lemma 5.4. *The adjoint of B satisfies the identity,*

$$B^* U = \frac{\partial}{\partial \nu} v = v_x(1).$$

Proof. The result follows by duality and (5.9). In particular,

$$(Bg, U)_H = (M^{-1} \mathcal{A} G g, M v) = (\mathcal{A} G g, v) =< g, G^* \mathcal{A} >=< g, \frac{\partial}{\partial \nu} v > .$$

Hence $< g, B^* U >=< g, \frac{\partial}{\partial \nu} v >$ and $B^* U = \frac{\partial}{\partial \nu} v = v_x(1)$.

□

Lemma 5.5. *Let $U(t) = e^{A_0 t} U(0)$. Then*

$$\int_0^T |u_{tx}(1,t)|^2 dt \leq C_T |U(0)|_H^2.$$

Remark 5.6. Note that the inequality in the lemma is a "hidden regularity" type of result. Finite energy data do not have traces u_{xt} defined on the boundary. However, the dynamics provide some regularizing effect.

Proof. We shall use the multiplier $x u_x$. Consider

$$\int_0^T (-\gamma u_{ttxx} + u_{tt} + u_{xxxx}, x u_x) dt = 0$$

with the boundary conditions:

$$u(0) = u_x(0) = 0 \text{ and } u_{xx}(1) = 0, -\gamma u_{ttx}(1) + u_{xxx}(1) = 0. \tag{5.10}$$

Integration by parts gives

$$(u_{xxxx}, x u_x) = (u_{xx}, u_{xx}) - (u_{xxx}, x u_{xx}) + < u_{xxx}, x u_x > - < u_{xx}, u_x >$$
$$-\gamma (u_{ttxx}, x u_x) = -\gamma < u_{ttx}, x u_x > + \gamma (u_{ttx}, x u_{xx} + u_x) - (u_{tt}, x u_x).$$

Adding the above, and integrating in time t yields

$$\int_0^T [(u_{xx}, u_{xx}) - (u_{xxx}, x u_{xx}) + < u_{xxx}, x u_x > - < u_{xx}, u_x > -\gamma < u_{ttx}, x u_x > -\gamma (u_{tx}, x u_{txx} + u_{tx})] dt$$

$$= \gamma (u_{tx}, x u_{xx} + u_x)|_0^T + \int_0^T (u_{tt}, x u_x) dt = \gamma (u_{tx}, x u_{xx} + u_x)|_0^T + (u_t, x u_x)|_0^T - \int_0^T (u_t, x u_{xt}) dt.$$

After applying the boundary conditions we have

$$\int_0^T [(u_{xx}, u_{xx}) - (u_{xxx}, xu_{xx}) - \gamma(u_{tx}, xu_{txx} + u_{tx})]dt = \gamma(u_{tx}, xu_{xx} + u_x)|_0^T.$$

Noting that

$$(u_{tx}, xu_{txx}) = 1/2(D_x(u_{tx}^2 x), 1) - 1/2(u_{tx}, u_{tx}),$$

we obtain

$$\int_0^T |u_{xt}(1)|^2 dt \le C|U(T)^2|_H + C|U(0)|_H^2 + \int_0^T |U(t)|^2 dt \le C_T|U(0)|_H^2$$

as desired. □

Step 2.
The lemma above translates via duality [24] into

$$\int_0^T |B^* e^{A_0^* t} U_0|^2 dt \le C|U_0|_H^2,$$

and the above condition is equivalent [24] to the boundedness of the operator L which proves Lemma 5.3. □

Step 3.
Using the variation of parameters formula we rewrite the original problem as

$$U(t) = e^{A_0 t} U(0) + (LN^* A_N P_2 U)(t)$$

where $U(t)$ is the solution of the original problem with $U = [u, v]$. The above is a fixed point problem which can be solved by the contraction mapping principle on $C(0, T; H)$. Here the method is identical to [23]. The key is the boundedness of L. The contraction constant is created by taking time T small. Since the problem is linear we can walk in finitely many steps. We then construct the continuous flow $U(t)$ on H. Ball's Theorem applied as in [23] implies the generation of the semigroup. The proof in the case $k_s = 0$ is thus completed. The case $k_m = 0$ is even simpler. This follows from the fact that $u_{tx}(1)$ is a lower order perturbation of the boundary operator $u_{ttx}(1)$. Since the regularity of solutions depends only on the principal of the operator, the term $k_s u_{tx}$ plays no role in the analysis.

□

5.1 Numerical Results for the Rayleigh Beam

The transcendental equations (3.16) and (3.17) for the Timoshenko beam apply for the Rayleigh beam with $g \to \infty$. In the monotone cases, the beam is stable and we see a vertical asymptote in the moment case in Figure 9. Indeed, asymptotic analysis reveals that with monotone moment feedback ($\bar{k}_s = k_m = k_s = 0$, $\bar{k}_m > 0$), for small $\bar{k}_m$,

$$\lambda_n \approx -\frac{1}{\bar{k}_m} \pm i\left(\frac{n\pi}{\sqrt{\gamma}}\right), \qquad n \in \mathbb{N},$$

and for large $\bar{k}_m$,

$$\lambda_n \approx -\frac{\bar{k}_m}{\gamma} \pm i\left(\frac{(2n-1)\pi}{2\sqrt{\gamma}}\right), \qquad n \in \mathbb{N}.$$

However, for monotone shear feedback ($\bar{k}_m = k_m = k_s = 0$, $\bar{k}_s > 0$), the eigenvalues do not line up along vertical asymptotes. Similar to the shear beam model, the eigenvalues above the real axis move along clockwise paths for the moment ($\bar{k}_m > 0$) feedback and counter-clockwise for the shear ($\bar{k}_s > 0$) feedback. We invite the reader to compare the spectral behaviors of the shear (Figure 7 and Rayleigh beams (Figure 9) with monotone feedback. They are similar, but the spectrum for the monotone moment feedback for the shear beam is qualitatively more like the spectrum for the Rayleigh beam with monotone shear feedback, and vice versa. This similarity is especially interesting when we note that both models are governed by essentially the same displacement PDE, (4.3) and (5.1). The difference between the models is in the boundary conditions.

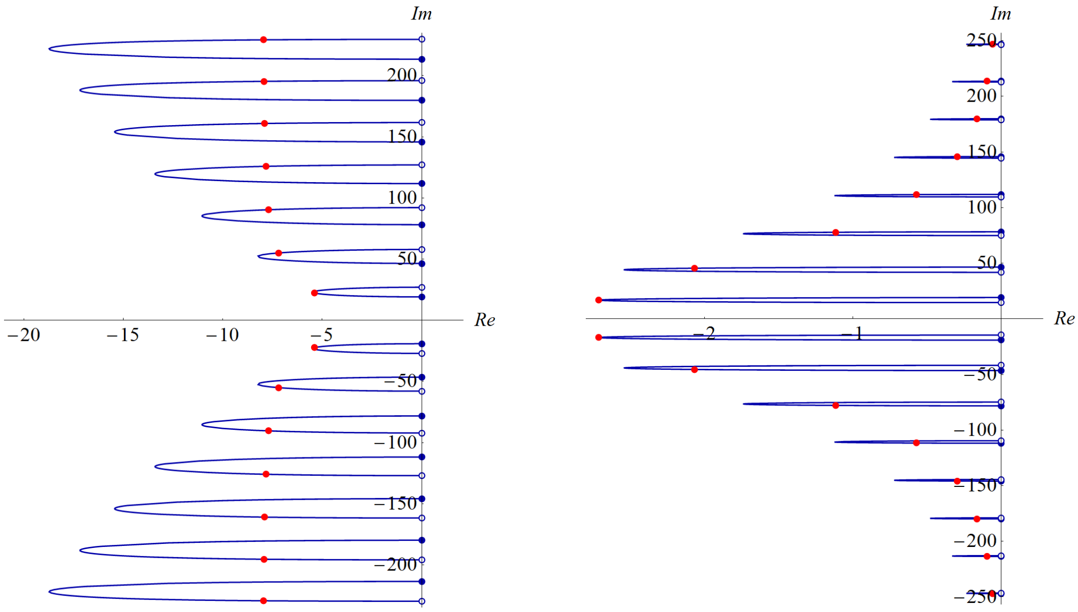

Figure 9. Portion of the spectrum for the Rayleigh beam with monotone moment (left, $\bar{k}_s = k_m = k_s = 0$, $\bar{k}_m = 0.15$, $\gamma = 0.01$) and shear (right, $\bar{k}_m = k_s = k_m = 0$, $\bar{k}_s = 3$, $\gamma = 0.01$) boundary conditions along with the paths that the eigenvalues take as the gain parameter increases from zero (disks) to infinity (open circles).

In the non-monotone case, the shear and Rayleigh models are even more dissimilar. Recall that the shear beam is stable, but [11] showed that the Rayleigh beam is unstable. Like Figure 1 in which $\gamma = 1$, with $\gamma = 0.01$, the eigenvalues are still clearly unstable as shown in Figure 10. However, the lower modes are stable and we have to ask ourselves, as we did in the Timoshenko case, if the unstable eigenvalues correspond to modes that are adequately modeled by a beam theory. Figure 11 shows the magnitude of the imaginary part of the first unstable eigenvalue as a function of $1/\gamma$. Unlike the Timoshenko case, the graph in Figure 11 appears to have polynomial growth, so for realistic values of γ, the unstable modes are all unlikely to be well-modeled by the theory. So, in the Rayleigh beam, even though there are an infinite number of unstable modes, all of the ones to which a beam theory may apply are all stable.

6 Conclusion

We have demonstrated very different stability and spectral behavior for four popular beam models that are, in some ways, all very similar models. All of the models are stable for monotone boundary conditions, but the margin of stability varies considerably between models. Recall that in the Timoshenko case, Figure 4, some of the eigenvalues remain extremely close to the imaginary axis. In the

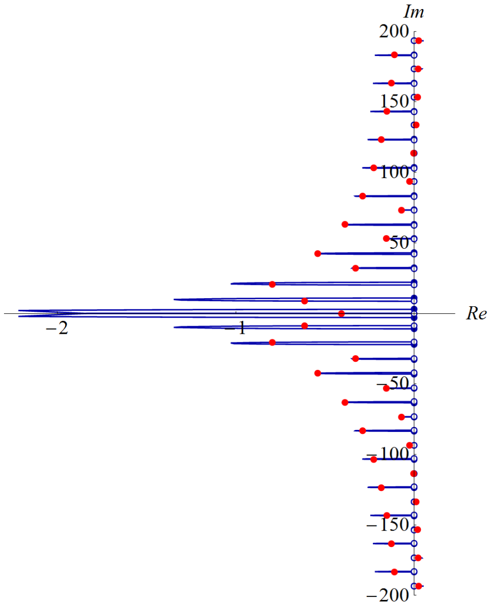

Figure 10. Portion of the spectrum for the Rayleigh beam with non-monotone moment ($\bar{k}_s = \bar{k}_m = k_s = 0$, $k_m = 5$,$\gamma = 0.1$) boundary conditions along with the paths that the eigenvalues take as the gain parameter increases from zero (disks) to infinity (open circles). Note that many of the higher modes are unstable.

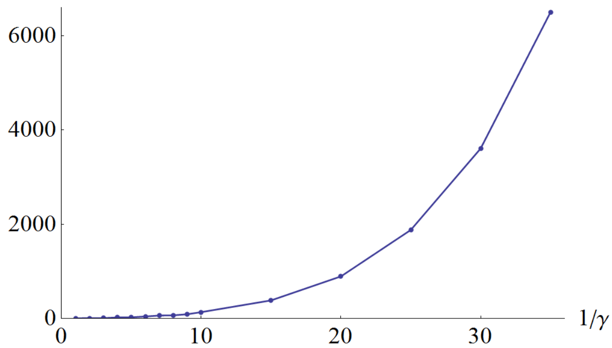

Figure 11. Graph of the magnitude of the smallest unstable eigenvalue (when $k_m > 0$) for the Rayleigh model as a function of $1/\gamma$.

case of non-monotone feedbacks, the shear and Euler-Bernoulli models have stable eigenvalues; the eigenvalues tend to lie along vertical asymptotes for the shear beam and on parabolic arcs for the Euler-Bernoulli beam. The Timoshenko and Rayleigh models, on the other hand, are unstable, but only for higher modes.

The discrepancies in the stability profiles of each model make physical interpretation very difficult. Remembering that beam models can only be applied for lower modes of vibration, it remains for further study to determine what actually happens to real beams with non-monotone moment or shear boundary conditions. This study could be done either by employing two- or three-dimensional elasticity solutions or by empirically testing beams in a laboratory. Finally, the current results apply only to beams, but other applications, such as boundary control of solar panels, may require similar analyses for plates or shells and the results in those cases may be even more variable due to the extra degrees of freedom in plate and shell models.

References

[1] Y. Gao, *Flexible Manipulators, Modeling, Analysis and Optimum Design, Intelligent Systems Series*, Associated Press/Elsevier Inc., Oxford, UK, 2012.

[2] M.O. Tokhi and A.K.M. Azad, *Flexible Robot Manipulators, Modelling, simulation and control*, The Institution of Engineering and Technology, London, UK 2008.

[3] F.-Y. Wang and Y. Gao, *Advanced Studies in Flexible Robotic Manipulators, Modeling, Design, Control and Applications, Series in Intelligent Control and Intelligent Automation*, Vol. 4, World Scientific Publishing Co., River Edge, NJ, 2003.

[4] W. Krabs and G.M. Sklyar, "On the Controllability of a Slowly Rotating Timoshenko Beam," *Journal for Analysis and its Applications*, 18 (1999), pp. 437-448.

[5] M.A. Shubov, "Generation of Gevrey class semigroup by non-selfadjoint Euler-Bernoulli beam model," Mathematical Methods in the Applied Sciences, vol. 29, issue 18, pp. 2181-2199.

[6] Z.H. Luo and B.Z. Guo, "Shear Force Feedback Control of a Single-Link Flexible Robot with a Revolute Joint," *IEEE Transactions on Automatic Control*, 42 (1997), pp. 53-65.

[7] G. Chen, S.G. Krantz, D.W. Ma, and C.E. Wayne, "The Euler-Bernoulli beam equation with boundary energy dissipation," in *Operator Methods for Optimal Control Problems*, S.J. Lee editor, New York, 1987, vol. 108.

[8] G. Chen, M. C. Delfour, A.M. Krall, and G. Payre, "Modeling, stabilization and control of serially connected beams," *SIAM J. Contr. Opt.*, 25 (1987), pp. 526-546.

[9] G. Guo and J. Wang and S. Yung, "On the C_0 semigroup generation and exponential stability resulting from a shear force feedback on a rotating beam", *Systems Control Letters*, vol 54, pp 557-575, 2005

[10] J. Kim and Y. Renardy,"Boundary Control of the Timoshenko Beam," *SIAM J. Control and Optimization*, Vol. 25, No. 6, Nov. 1987.

[11] C. Guiver and M. Opmeer, "Non-dissipative boundary feedback for Rayleigh and Timoshenko beams," *Systems & Control Letters*, vol. 59, no. 9, pp. 578-586, 2010.

[12] B. Belinskiy and I. Lasiecka, "Gevrey's and Trace Regularity of a Semigroup Associated with Beam Equation and Non-Monotone Boundary Conditions," *Journal of Mathematical Analysis and Applications*, 332 (2007), pp. 137-154.

[13] I. Lasiecka and D. Toundykov, "Semigroup generation and "hidden" trace regularity of a dynamic plate with non-monotone boundary feedbacks," *Communications in Mathematical Analysis*, Invited Volume for Peter Lax, Vol 8, No. 1, (2010), pp. 1-37.

[14] I. Lasiecka, R. Marchand, and T. McDevitt, "Boundary Control and Hidden Trace Regularity of a Semigroup Associated with a Beam Equation and Non-Dissipative Boundary Conditions," *Journal of Dynamical Systems and Applications*, 21 (2012), pp. 467-490.

[15] S. Han, H. Benaroya, and T. Wei, "Dynamics of Transversely Vibrating Beams Using Four Engineering Theories," *Journal of Sound and Vibration*, 225 (1999), pp. 935-988.

[16] L. Majkut, "Free and Forced Vibrations of Timoshenko Beams Described by a Single Difference Equation," *Journal of Theoretical and Applied Mechanics*, 47 (2009), pp. 193-210.

[17] W.J.W. Rankine, "A Manual of Applied Mechanics," Richard Griffin and Co., pp. 342-344.

[18] Lord J.W. Rayleigh, *The Theory of Sound*, Volume I and II, Dover, New York, 1945.

[19] Timoshenko, S.P. "On the correction for shear of the differential equation for transverse vibration of prismatic bars," *Phil. Mag.*, 41, pp. 744-746.

[20] M. A. Horn and I. Lasiecka, "Asymptotic behavior with respect to thickness of boundary stabilizing feedback for the Kirchoff plate," *Journal of Differential Equations,* Vol 114, (1994), pp. 396-433.

[21] I. Lasiecka, "Boundary Stabilization of a 3-dimensional structural acoustic model," *J. Math. Pure Applic,* Vol 78, (1999), pp. 203-232.

[22] I. Lasiecka, *Mathematical Control Theory of Coupled PDE's*, CBMS-SIAM-NSF- Lecture Notes, SIAM, 2002.

[23] W. Desh, I. Lasiecka, and W. Shappacher, "Feedback boundary control problems for linear semigroups," *Israel Journal of Mathematics,* Vol. 51, no. 3, pp. 177-207, 1985.

[24] I. Lasiecka and R. Triggiani, *Control Theory for Partial Differential Equations, vol I, vol II.* Encyclopedia of Mathematics, Cambridge University Press. 2000

[25] I. Chueshov and I. Lasiecka, *Von Karman Evolutions.* Springer-Verlag, 2010.

Author information

Richard J. Marchand, Department of Mathematics, Slippery Rock University, Slippery Rock, PA 16057, USA.
E-mail: richard.marchand@sru.edu

Timothy J. McDevitt, Department of Mathematical and Computer Sciences, Elizabethtown College, Elizabethtown, PA 17022-2290, USA.
E-mail: mcdevittt@etown.edu

Received: February 2, 2013

Accepted: April 15, 2013